

# Spintronics meets density matrix renormalization group: Nonclassical magnetization reversal and entanglement growth due to current-pulse-driven quantum spin torque

Marko D. Petrović,<sup>1</sup> Adrian E. Feiguin,<sup>2</sup> Petr Plecháč,<sup>3</sup> and Branislav K. Nikolić<sup>1,\*</sup>

<sup>1</sup>*Department of Physics and Astronomy, University of Delaware, Newark DE 19716, USA*

<sup>2</sup>*Department of Physics, Northeastern University, Boston, MA 02115, USA*

<sup>3</sup>*Department of Mathematical Sciences, University of Delaware, Newark, DE 19716, USA*

We introduce time-dependent density matrix renormalization group (tDMRG) as a fully quantum framework for spin-transfer torque (STT), and apply it to understand if recently discovered quantum STT in spin valves at ultralow temperature can lead to magnetization reversal. The conventional Slonczewski-Berger STT—where the magnetization is viewed as a classical vector described by the Landau-Lifshitz-Gilbert equation—occurs only when spin-polarization of injected electrons and localized spins are *noncollinear*. Conversely, quantum STT occurs when these vectors are *collinear but antiparallel*, thereby requiring a fully quantum treatment of *both* electrons and localized spins. Using tDMRG, we simulate time evolution of a many-body quantum state of electrons and localized spins, where the former are injected as spin-polarized current pulse from fermionic leads while the latter comprise a quantum Heisenberg ferromagnetic metallic (FM) spin- $\frac{1}{2}$  XXZ chain that can also be viewed as a Kondo-Heisenberg chain. The quantum STT reverses the direction of localized spins, but without rotation from the initial orientation, when the number of injected electrons exceeds the number of localized spins. Such *nonclassical reversal* is highly inhomogeneous across the FM chain and accompanied by reduction of the magnetization associated with localized spins, even to zero at specific locations. This is because quantum STT driven nonequilibrium dynamics generates *highly entangled* nonequilibrium many-body state of all flowing and localized spins, despite starting from initially separable quantum state of a mundane FM, thereby leading to true decoherence of each localized spin subsystem. The global entanglement growth differentiates between quantum and conventional STT since in the former case it nearly reaches the maximum possible value.

**Introduction.**—The conventional spin-transfer torque (STT) has been at the forefront of basic [1] and applied [2] research in spintronics since the seminal theoretical predictions of Slonczewski [3] and Berger [4]. Its key requirement is that spin-polarization of conduction electrons injected into a ferromagnetic metal (FM) must be *noncollinear* to FM magnetization, as illustrated in Fig. 1(b). Thus, it came as a great surprise when current-driven magnetization dynamics was recently observed at ultralow  $T \sim 1$  K temperatures [5, 6] in spin valves FM-polarizer/normal-metal/FM-analyzer with *collinear* magnetizations. Although thermal fluctuations of magnetization can create the required noncollinearity in spin valves (or magnetic tunnel junctions) at room temperature [6], they are frozen at ultralow temperatures of the experiment in Ref. [5]. Thus, the effect observed in Ref. [5] was dubbed “quantum STT” [6] and believed to be dissociated from conventional STT.

The standard model [1] of conventional STT involves localized magnetic moments  $\mathbf{M}_i$ , viewed as classical vectors of fixed length, which interact with a nonequilibrium electronic spin density  $\mathbf{s}_i$ , computed by some steady-state [7, 8] or time-dependent [9] quantum transport formalism, that is fed into the Landau-Lifshitz-Gilbert (LLG) equation [10]. Thus, in the context of the quantum STT setup of Ref. [5] where the conventional Slonczewski-Berger STT  $\propto \mathbf{s}_i \times \mathbf{M}_i \equiv 0$  is *identically zero*, as illustrated in Fig. 1(a),(c), this formalism based on classical dynamics of localized spins becomes inapplicable. Surprisingly, despite a long history of STT,

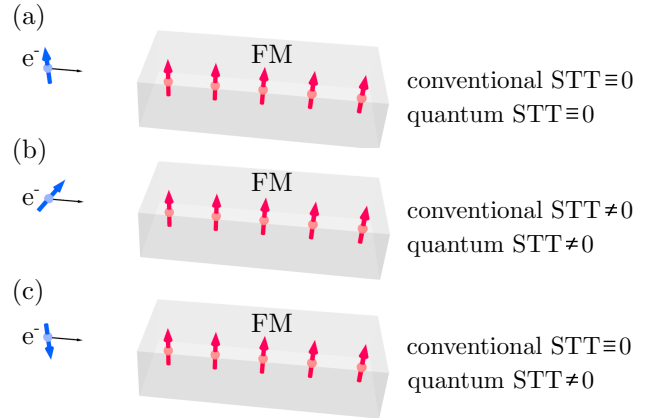


FIG. 1. Illustration of three types of geometries of flowing electron spin (blue arrow) with respect to localized spins (red arrows) within FM-analyzer layer: (a) parallel; (b) non-collinear; and (c) antiparallel. The conventional STT [1, 3, 4] is nonzero only in (b), while quantum STT [5] is nonzero in both (b) and (c). Blue and red arrows represent expectation values of the corresponding quantum-mechanical spin operators. For conventional STT, red arrows are modeled as classical vectors of fixed length [1, 9, 10].

an established fully quantum-mechanical framework for coupled dynamics of localized spins and flowing electron spins, as well as transfer of spin angular momentum between them, is still lacking [5, 6].

A handful of recent theoretical studies [11–13] have

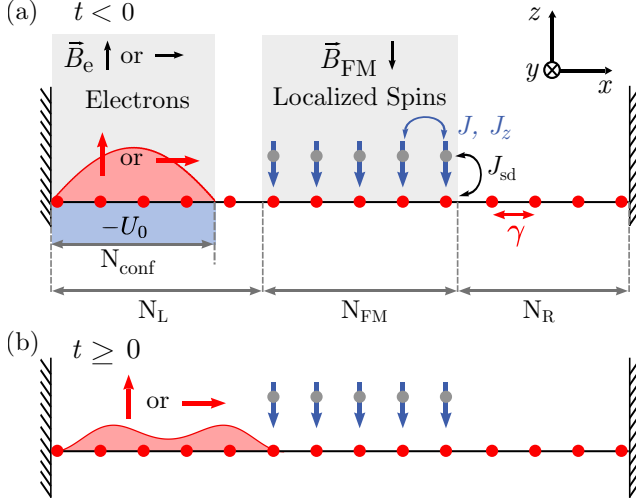


FIG. 2. Schematic view of a two-terminal setup for tDMRG calculations where 1D tight-binding chain (blue dots) of  $N = 75$  sites, with electron nearest-neighbor hopping  $\gamma$  between all sites, hosts  $N_{\text{FM}} = 5$  localized spins- $\frac{1}{2}$  (red arrows) comprising a ferromagnetic quantum Heisenberg XXZ chain. First  $N_L = 35$  sites within the left fermionic lead also include  $N_{\text{conf}} = 10$  sites where the confining potential  $V$  is applied to  $N_e \in \{1, 5, 8\}$  electrons filling those sites. For  $t < 0$ , external magnetic fields  $\mathbf{B}_e$  and  $\mathbf{B}_{\text{FM}}$  polarize electron spins along the  $+z$ -axis or  $+x$ -axis and localized spins along the  $-z$ -axis, respectively. For  $t \geq 0$ , both magnetic fields and the confining potential are switched off, so that electrons spread from left to right, as also animated by the movie in the SM [19].

offered insights into possible microscopic mechanisms of quantum STT. However, they rely on either: (i) a mapping of original operators of localized spins to bosonic operators and an additional approximation that does not allow to track the time evolution of localized spins that deviates too far from the initial orientation set by the anisotropy axis [11, 12]; or (ii) they consider only one injected spin-polarized electron [13], which is insufficient to reverse many localized spins because of demand posed by angular momentum conservation.

In this study, we introduce the adaptive time-dependent density matrix renormalization group (tDMRG) [14–17] as a numerically (nearly) exact framework capable of describing quantum and conventional STT on the same footing. Since this simulation method works directly with the original quantum-mechanical operators of the localized spins, it can capture reversal of localized spins due to STT which is highly sought in spintronic applications [1, 2, 8]. We demonstrate this by applying the tDMRG to a one-dimensional (1D) setup depicted in Fig. 2 where quantum Heisenberg FM spin- $\frac{1}{2}$  XXZ chain is attached to the left (L) and right (R) fermionic leads modeled as 1D tight-binding chains of finite length. The *nonzero* electron hopping between the sites of the XXZ chain means that FM

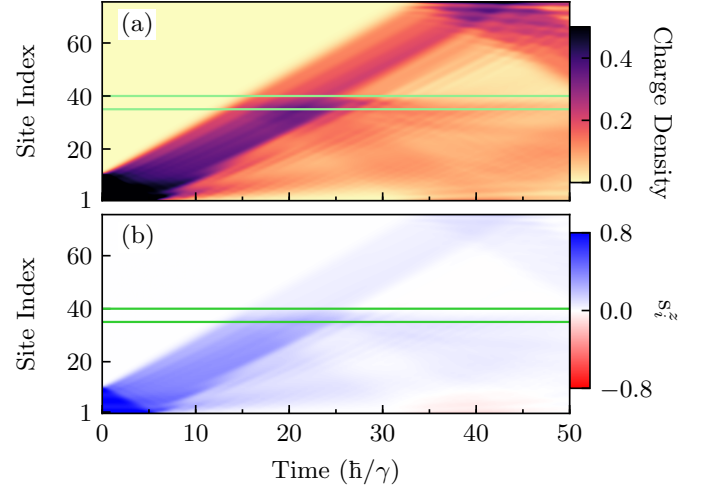


FIG. 3. Spatio-temporal profiles of electronic (a) charge density and (b) spin- $z$  density for spin-polarized current pulse composed of  $N_e = 8$  electrons injected into the FM region in Fig. 2. The green horizontal lines in both panels mark the first and the last localized spin of the FM region. Electrons are initially ( $t < 0$ ) spin-polarized along the  $+z$ -axis, while localized spins are polarized along the  $-z$ -axis. The strength of  $sd$  exchange interaction between electron spin and localized spins is  $J_{sd} = 0.5\gamma$ . Both panels are animated as a movie in the SM [19] for  $J_{sd} = 0.5\gamma$  and  $J_{sd} = 2.0\gamma$ .

chain models *metallic* FM-analyzer layer that is receiving STT. From the viewpoint of the physics of strongly correlated electrons, this can also be interpreted as Kondo-Heisenberg chain [18] sandwiched by fermionic leads, with ferromagnetic exchange interaction between both the localized spins and those spins and 1D electron gas.

The role of the FM-polarizer layer is simulated by filling the L lead with  $N_e$  electrons (one per site), which are spin-polarized in a desired direction by applying an external magnetic field in that direction. They are also confined into a quantum well for times  $t < 0$ , as illustrated in Fig. 2(a). By removing the confining potential for times  $t \geq 0$ , electrons spread into the region of the localized FM moments, as shown in Fig. 3 and animated in the movie in the Supplemental Material (SM) [19]. Thus, this procedure mimics injection of a spin-polarized current pulse often employed in STT-operated spintronic devices [1, 2, 8]. Prior to explaining our principal results in Figs. 3–6 for the STT-driven quantum dynamics of the local magnetization across the FM chain, we first introduce useful concepts and necessary notation.

*Model Hamiltonians and methods.*—The setup illustrated in Fig. 2 is a 1D chain of  $N$  sites where electrons and localized spins are described by the Hamiltonian

$$\hat{H} = \hat{H}_e + \hat{H}_{\text{lspins}} + \hat{H}_{e-\text{lspins}} + \hat{H}_{V,\mathbf{B}}(t < 0). \quad (1)$$

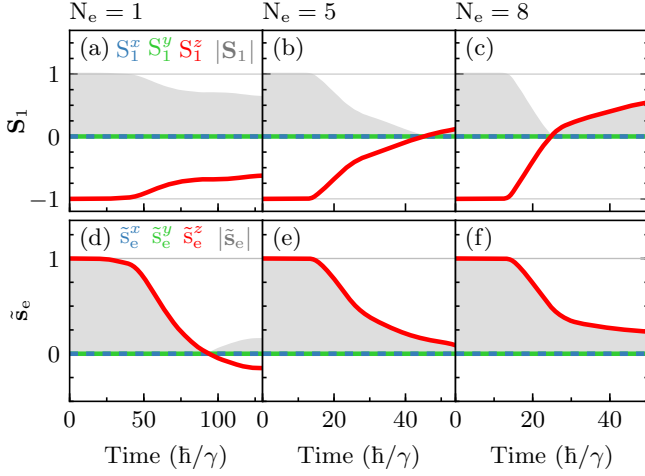


FIG. 4. Time evolution of the expectation value of first localized spin  $\mathbf{S}_1 = (S_1^x, S_1^y, S_1^z)$  and the purity  $|\mathbf{S}_1|$  of its quantum state (gray background) for a different number of injected electrons which are initially spin-polarized along the  $+z$ -axis: (a)  $N_e = 1$ ; (b)  $N_e = 5$ ; and (c)  $N_e = 8$ . Panels (d)–(f) plot average electron spin expectation value,  $\tilde{\mathbf{s}}_e = \mathbf{s}_e/N_e$ , and purity,  $|\tilde{\mathbf{s}}_e|$ . The  $sd$  exchange interaction between electron spin and localized spins is  $J_{sd} = 0.5\gamma$ . Panels (c) and (f) are animated as a movie in the SM for  $J_{sd} = 0.5\gamma$  and  $J_{sd} = 2.0\gamma$ .

The tight-binding Hamiltonian for electrons

$$\hat{H}_e = -\gamma \sum_{i=1}^{N-1} \left( \hat{c}_{i\uparrow}^\dagger \hat{c}_{i+1\uparrow} + \hat{c}_{i\downarrow}^\dagger \hat{c}_{i+1\downarrow} + \text{h.c.} \right), \quad (2)$$

operates on all  $N = 75$  sites, where  $\hat{c}_{i\sigma}^\dagger$  ( $\hat{c}_{i\sigma}$ ) creates (annihilates) an electron with spin  $\sigma = \uparrow, \downarrow$  on site  $i$ . The nearest-neighbor (NN) hopping parameter  $\gamma$  sets a unit of energy. Each site hosts one of the four possible electronic quantum states—empty  $|0\rangle$ , spin-up  $|\uparrow\rangle = \hat{c}_{i\uparrow}^\dagger|0\rangle$ , spin-down  $|\downarrow\rangle = \hat{c}_{i\downarrow}^\dagger|0\rangle$ , and doubly occupied  $|\uparrow\downarrow\rangle = \hat{c}_{i\uparrow}^\dagger \hat{c}_{i\downarrow}^\dagger|0\rangle$ —from which one can construct  $4^N$  many-body states that span the Fock space  $\mathcal{F}_e$ . The operators for the total number of electrons  $\hat{N}_e = \sum_{i=1}^N \hat{n}_i$  and total electron spin along the  $z$ -axis  $\hat{s}_e^z = \sum_{i=1}^N \hat{s}_i^z$  are given by sums of local (per-site) charge and spin density operators,  $\hat{n}_i = \sum_{\sigma=\{\uparrow,\downarrow\}} \hat{c}_{i\sigma}^\dagger \hat{c}_{i\sigma}$  and  $\hat{s}_i^z = \sum_{\sigma=\{\uparrow,\downarrow\}} (-1)^{\sigma-1/2} \hat{c}_{i\sigma}^\dagger \hat{c}_{i\sigma}$ , respectively. Out of  $N = N_L + N_{\text{FM}} + N_R$  sites in Fig. 2, the first  $N_L = 35$  belong to the L fermionic lead and the last  $N_R = 35$  belong to the R fermionic lead. The middle  $N_{\text{FM}} = 5$  sites host localized spins whose mutual interaction is described by ferromagnetic XXZ spin- $\frac{1}{2}$  quantum Heisenberg Hamiltonian

$$\hat{H}_{\text{spins}} = - \sum_{i=1}^{N_{\text{FM}}-1} \left[ J_z \hat{S}_i^z \cdot \hat{S}_{i+1}^z + J \left( \hat{S}_i^x \cdot \hat{S}_{i+1}^x + \hat{S}_i^y \cdot \hat{S}_{i+1}^y \right) \right]. \quad (3)$$

Here  $\hat{\mathbf{S}}_i$  is the spin- $\frac{1}{2}$  operator located on lattice site  $i$ ; and the NN exchange interactions between localized

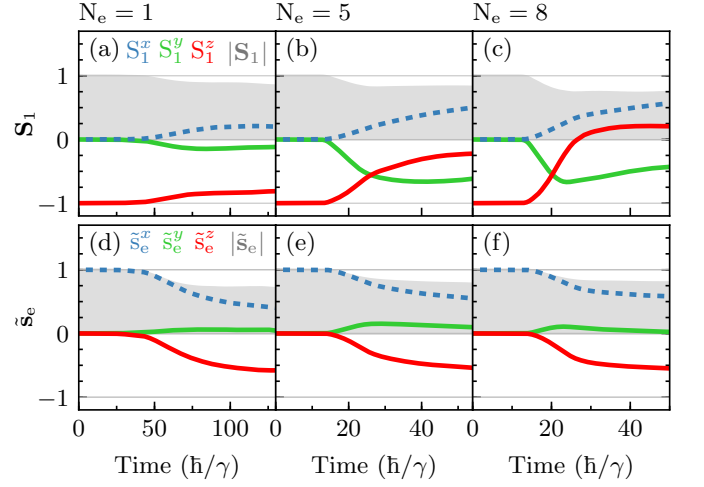


FIG. 5. Panels (a)–(f) are counterparts of Fig. 4(a)–(f), but for injected electrons which are spin-polarized at  $t < 0$  along the  $+x$ -axis. This creates a noncollinear geometry of flowing and localized spins, as required for conventional STT [1].

spins are  $J = 0.1\gamma$  and  $J_z = 0.1005\gamma$ , thereby including anisotropy along the  $z$ -axis. The  $2^{N_{\text{FM}}}$ -dimensional Hilbert space of all localized spins is constructed as  $\mathcal{H}_{\text{lspins}} = \mathcal{H}_1 \otimes \mathcal{H}_2 \otimes \dots \otimes \mathcal{H}_{N_{\text{FM}}}$ . Thus, the total Hamiltonian in Eq. (1) acts on the space  $\mathcal{F}_e \otimes \mathcal{H}_{\text{lspins}}$ , where the interaction between conduction electron spins and localized spins is described by

$$\hat{H}_{e-\text{lspins}} = - \sum_{i=N_L+1}^{N_{\text{FM}}} J_{sd} \left( \hat{s}_i^x \cdot \hat{S}_i^x + \hat{s}_i^y \cdot \hat{S}_i^y + \hat{s}_i^z \cdot \hat{S}_i^z \right). \quad (4)$$

Here  $J_{sd} = 0.5\gamma$  (movie in the SM [19] shows additional case with  $J_{sd} = 2.0\gamma$ ) is interpreted as either  $sd$  [1] or Kondo ferromagnetic exchange [18] interaction in the fields of spintronics or strongly correlated electrons, respectively.

For the purpose of preparing a many-electron spin-polarized current pulse, we employ the following term

$$\begin{aligned} \hat{H}_{V,\mathbf{B}}(t < 0) = & -V \sum_{i=1}^{N_{\text{conf}}} \left( \hat{c}_{i\uparrow}^\dagger \hat{c}_{i\uparrow} + \hat{c}_{i\downarrow}^\dagger \hat{c}_{i\downarrow} \right) \\ & - \sum_{i=1}^{N_{\text{conf}}} g\mu_B \hat{\mathbf{S}}_i \cdot \mathbf{B}_e - \sum_{i=N_L+1}^{N_{\text{FM}}} g\mu_B \hat{\mathbf{S}}_i \cdot \mathbf{B}_{\text{FM}}, \end{aligned} \quad (5)$$

in Eq. (1) which acts at times  $t < 0$  and is used only once to initialize the system. The first term in Eq. (5) is a confining on-site potential of magnitude  $V = 10\gamma$  acting within the first  $N_{\text{conf}} = 10$  sites of  $N_L = 35$  sites of the L fermionic lead, as illustrated in Fig. 2(a). In addition, the second term in Eq. (5) polarizes, via an external magnetic field  $|g\mu_B \mathbf{B}_e| = 100\gamma$ , the confined electrons along the  $+z$ -axis for the collinear setup of quantum STT analyzed in Figs. 3, 4 and 6(a), as well as in the movie in the

SM [19]; or spin-polarizes them along the  $+x$ -axis for the noncollinear setup of conventional STT [1] analyzed in Figs. 5 and 6(b)–(d). The third term in Eq. (5) is employed to polarize the localized spins along the  $-z$ -axis using an external magnetic field  $|g\mu_B\mathbf{B}_{\text{FM}}| = 100\gamma$ . The electron gyromagnetic ratio is denoted by  $g$ , and  $\mu_B$  is the Bohr magneton.

For  $t \geq 0$ ,  $\hat{H}_{V,B} \equiv 0$  so that spin-polarized conduction electrons spread out from the region of  $N_{\text{conf}}$  sites and are injected into the FM chain. This process is illustrated in Fig. 2(b), while the local charge and spin- $z$  densities are computed numerically in Fig. 3 and animated in the movie in the SM [19]. Since fermionic leads are not semi-infinite as in the usual quantum transport calculations [9], the many-body system composed of conduction electrons and localized spins can be evolved only for a limited time before electrons are backscattered by the right boundary which breaks L $\rightarrow$ R current flow. For example, in Fig. 3 such backscattering occurs at  $t \simeq 40\hbar/\gamma$  for  $N_e = 8$  injected electrons. Nevertheless, the quantum dynamics of flowing electron spins and localized spins captured by tDMRG before the boundary reflection is fully equivalent to that in an open quantum system.

*Quantum STT in collinear geometry.*—In the collinear setup [5, 6] of quantum STT, the spin-polarization of the injected conduction electrons is collinear but antiparallel to that of the localized spins at  $t = 0$ . In the sector  $N_e = 0$ , the many-body quantum state  $|\Psi(t)\rangle$  for  $t \geq 0$  within  $\mathcal{F}_e \otimes \mathcal{H}_{\text{spins}}$  space is trivially  $|\Psi(t)\rangle = |\text{vac}\rangle \otimes |G\rangle$  where the first factor of such separable quantum state is the electron vacuum state  $|\text{vac}\rangle \in \mathcal{F}_e$  and the second factor  $|G\rangle = |\downarrow_1 \dots \downarrow_{N_{\text{FM}}}\rangle \in \mathcal{H}_{\text{spins}}$  is the ground state of the FM chain. The sector  $N_e = 1$  has been studied for an infinite ( $N_{\text{FM}} \rightarrow \infty$ ) metallic FM chains long before [20] theoretical predictions for STT, but with the focus on magnetic polarons as the bound state of the injected electron and low-energy excitations (spinons or magnons) of all localized spins. In such a case, and for a FM chain [13] of finite length, we find  $|\Psi(t \geq 0)\rangle = c_0(t)|\text{orb}\rangle \otimes |\uparrow_e\rangle \otimes |G\rangle + c_1(t)|\text{orb}\rangle \otimes |\downarrow_e\rangle \otimes |\uparrow_1 \dots \downarrow_{N_{\text{FM}}}\rangle + \dots + c_{N_{\text{FM}}}(t)|\text{orb}\rangle \otimes |\downarrow_e\rangle \otimes |\downarrow_1 \dots \uparrow_{N_{\text{FM}}}\rangle$ . This superposition is constructed by including *all possible states* allowed by the conservation of the  $z$ -component of total spin,  $[\hat{H}, \hat{S}_e^z + \hat{S}_{\text{spins}}^z] = 0$ , where  $\hat{S}_{\text{spins}}^z = \hat{S}_1^z + \dots + \hat{S}_{N_{\text{FM}}}^z$ . Here  $|\text{orb}\rangle$  is orbital state of a single injected electron, and the coefficients  $c_0(t), \dots, c_{N_{\text{FM}}}(t)$  studied in Ref. [13] can be much more complicated than those for magnons (or spinons) in an infinite FM chain [20].

The quantum state  $|\Psi(t)\rangle$  also defines the pure state density matrix  $|\Psi(t)\rangle\langle\Psi(t)|$ . Since such state for  $N_e \geq 1$  is a sum of separable states and, therefore, entangled, the quantum state of subsystems must be described by the reduced density matrix [21]. This is exemplified by

$$\hat{\rho}_1 = \text{Tr}_{\text{other}} |\Psi(t)\rangle\langle\Psi(t)| = \frac{1}{2} [\hat{I} + \mathbf{S}_1 \cdot \hat{\boldsymbol{\sigma}}], \quad (6)$$

which is the density matrix of the first localized spin (at site  $N_L + 1$  in Fig. 2), obtained by partial trace over all states within  $\mathcal{F}_e \otimes \mathcal{H}_{\text{spins}}$  that are not in  $\mathcal{H}_1$ . Here  $\hat{I}$  is the unit  $2 \times 2$  matrix and  $\hat{\boldsymbol{\sigma}} = (\hat{\sigma}_x, \hat{\sigma}_y, \hat{\sigma}_z)$  is the vector of the Pauli matrices. The magnitude  $|\mathbf{S}_1|$  of the expectation value of localized spin,  $\mathbf{S}_1 = \text{Tr}[\hat{\rho}_1 \hat{\boldsymbol{\sigma}}]$ , also serves as *purity* [21] specifying whether its quantum state is fully ( $|\mathbf{S}_1| = 1$ ) or partially ( $0 < |\mathbf{S}_1| < 1$ ) coherent. We use label  $O \equiv \langle \hat{O} \rangle$  for the expectation value of an operator  $\hat{O}$  in a pure many-body state of the total system electrons plus localized-spins or in a mixed quantum state of a relevant (depending on observable  $\hat{O}$ ) subsystem. Thus, *true* decoherence (i.e., decoherence that cannot be attributed to any classical noise [22]) due to many-body entanglement can lead to reduction of local and total magnetization,  $\mathbf{M}_i = g\mu_B \mathbf{S}_i$  and  $\mathbf{M} = \sum_{i=N_L+1}^{N_{\text{FM}}} g\mu_B \mathbf{S}_i$ , respectively, because of reduction of  $\mathbf{S}_i$  expectation values. This is obviously forbidden in classical magnetization dynamics described by the LLG equation [7, 9, 10].

The time evolution of  $\mathbf{S}_1(t)$  is shown in Fig. 4(a)–(c) for  $N_e = 1, 5, 8$  injected electrons, respectively; as well as in the movie in the SM [19] for all  $\mathbf{S}_i(t)$  using  $N_e = 8$ . Due to spin angular momentum conservation, only  $S_i^z(t) \neq 0$ . The magnetization reversal sought in spintronic applications [1, 2], where  $S_i^z(t)$  evolves from  $S_i^z = -1$  at  $t = 0$  to  $S_i^z > 0$  at some later time  $t > 0$ , occurs only when  $N_e > N_{\text{FM}}$ . The reversal is *nonclassical* since  $S_i^x(t) = S_i^y(t) \equiv 0$ , unlike classical magnetization reversal [1, 8, 10] where  $\mathbf{M}_i$  vectors must rotate away from the  $-z$ -axis to reach the  $+z$ -axis. The decoherence of localized spin states makes the reversal inhomogeneous (see movie in the SM [19]) because localized spins away from the L-lead/FM-chain interface have smaller  $|\mathbf{S}_i|$  or  $S_i^z$  can remain negative. The decoherence can be partially suppressed and all localized spins reversed by increasing  $J_{sd}$ , despite larger  $J_{sd}$  concurrently enhancing reflection of the current pulse at the L-lead/FM-chain interface (see the movie in the SM [19]).

The spin expectation value per electron,  $\tilde{\mathbf{s}}_e = \mathbf{s}_e/N_e$ , plotted in Fig. 4(d)–(f) shows that, due to many-body entanglement, electron spin states decohere with purity  $|\tilde{\mathbf{s}}_e| < 1$ . In the sector  $N_e = 1$ , we can understand the quantum dynamics of electron and localized spins from analytical calculations for a toy model. Suppose, that a single spin-up electron is injected into the FM region with two localized spins, so that total spin- $z$  is  $s_e^z + S_{\text{spins}}^z = -1$ ;  $|\Psi(t=0)\rangle = |\text{orb}\rangle \otimes |\uparrow_e\rangle \otimes |\downarrow_1 \downarrow_2\rangle$ ; and  $|\Psi(t \geq 0)\rangle = c_0(t)|\text{orb}\rangle \otimes |\uparrow_e\rangle \otimes |\downarrow_1 \downarrow_2\rangle + c_1(t)|\text{orb}\rangle \otimes |\uparrow_1 \downarrow_2\rangle + c_2(t)|\text{orb}\rangle \otimes |\downarrow_e\rangle \otimes |\downarrow_1 \uparrow_2\rangle$ . If we assume for simplicity  $c_0(t) = c_1(t) = c_2(t) = 1/\sqrt{3}$  (in numerically exact calculations [13], these coefficients are time-dependent and  $|c_0(t)| \gg |c_1(t)|, |c_2(t)|$ ), we obtain three spin density matrices via Eq. (6):  $\hat{\rho}_e = (\hat{I} + \tilde{\mathbf{s}}_e \cdot \hat{\boldsymbol{\sigma}})/2$  for electron spin;  $\hat{\rho}_1 = (\hat{I} + \mathbf{S}_1 \cdot \hat{\boldsymbol{\sigma}})/2$  for the first localized spin; and  $\hat{\rho}_2 = (\hat{I} + \mathbf{S}_2 \cdot \hat{\boldsymbol{\sigma}})/2$  for the second localized spins. They are specified by three vectors,  $\tilde{\mathbf{s}}_e = \mathbf{S}_1 = \mathbf{S}_2 = (0, 0, -1/3)$ ,

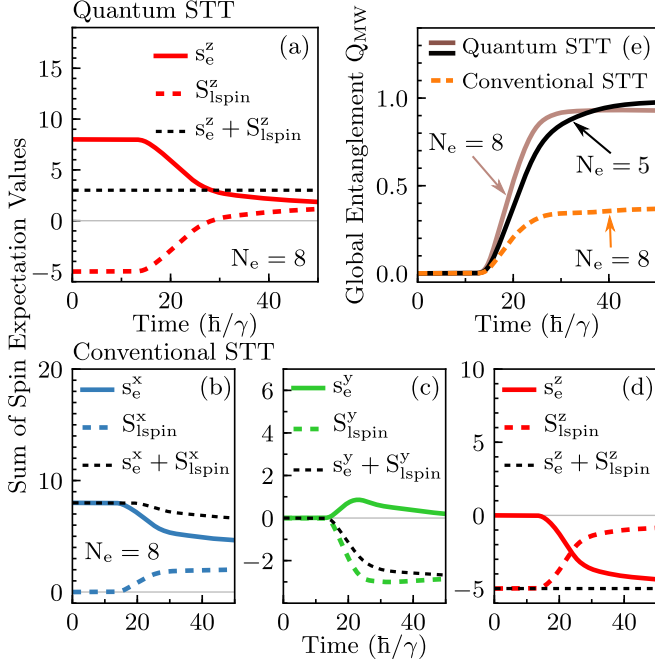


FIG. 6. (a) Time evolution of the sum of spin expectation values for all injected  $N_e = 8$  electrons  $s_e^z(t)$ , as well as of all  $N_{\text{FM}} = 5$  localized spins  $S_{\text{spins}}^z(t)$ , for collinear and antiparallel setup of quantum STT analyzed in Fig. 4(c),(f). The same time evolution, but for noncollinear setup of conventional STT analyzed in Fig. 5(c),(f), is shown in panels (b)–(d). The  $z$ -component of total spin is manifestly conserved (dashed blacked line) in panels (a) and (d). Panel (e) plots time evolution of global entanglement measure in Eq. (7) for electron-spins plus localized-spins multipartite system.

showing that all three spins are in partially coherent quantum states while the total spin- $z$  angular momentum remains conserved,  $\tilde{s}_e^z + S_1^z + S_2^z = -1$ .

*Conventional STT in noncollinear geometry.*—For the sake of comparison, we examine in Fig. 5 conventional STT in a noncollinear geometry where injected electrons are spin-polarized along the  $+x$ -axis while localized spins are polarized along the  $-z$ -axis. Although this has been considered [5, 6] as a completely different situation from quantum STT in a collinear geometry, the state  $|\rightarrow_e^x\rangle$  in quantum language corresponds to the injection of a superposition of spin-up and spin-down states,  $|\rightarrow_e^x\rangle = (|\uparrow_e\rangle + |\downarrow_e\rangle)/\sqrt{2}$ . In this case, we find in Fig. 5(a)–(c) that the localized spins always rotate,  $S_i^x \neq 0$  and  $S_i^y \neq 0$ , away from the easy  $z$ -axis for  $t \geq 0$  akin to classical localized spins [1, 8, 10]. However,  $|\mathbf{S}_1| < 1$  in Fig. 5(a)–(c) signifies the same decoherence due to many-body entanglement found for quantum STT in Fig. 4. Nevertheless, asymptotic value of global entanglement reached is much smaller in conventional STT than in the case of quantum STT [Fig. 6(e) and discussion below].

*What is “transferred” in spin-transfer torque?*—The conventional STT is commonly computed using some type of single-particle steady-state quantum transport formalism [7, 8, 23] to obtain the nonequilibrium electron spin density  $\mathbf{s}_i$  injected into the FM-analyzer. Due to noncollinearity between  $\mathbf{s}_i$  and the classical magnetization  $\mathbf{M}$  of the FM-analyzer, contributions to  $\mathbf{s}_i$  from propagating states oscillate as a function of position without decaying. Nevertheless, the transverse (with respect to  $\mathbf{M}$ ) component of  $\mathbf{s}_i$  is brought to zero within  $\sim 1$  nm away from the normal-metal/FM-analyzer interface by averaging over propagating states with different incoming momenta  $\hbar\mathbf{k}$  because the frequency of spatial oscillations rapidly changes with  $\mathbf{k}$  [23]. The angular dependence of  $\text{STT} \propto \sum_i \mathbf{s}_i \times \mathbf{M}$  can be fed [7, 8] into the LLG calculations which often consider only the macrospin [1, 10, 24]  $\mathbf{M} = \sum_i \mathbf{M}_i$ . Thus, in this picture the microscopic mechanism of how spin angular momentum is transferred from electron subsystem to magnetization remains hidden. The tDMRG unveils such mechanism in Fig. 6(a) for quantum STT, as well as in Fig. 6(b)–(c) for conventional STT, where the total spin of all electrons  $s_e^z(t)$  decays in time while the total spin of all localized spins  $S_{\text{spins}}^z(t)$  increases as injected flowing spins try to align localized spins in the same direction. Figure 6(a),(d) also validates our calculations by confirming that  $s_e(t) + S_{\text{spins}}^z(t)$  remains constant, as expected from the conservation law  $[\hat{H}, \hat{s}_e^z + \hat{S}_{\text{spins}}^z] = 0$ . Due to the complex superposition of many-body states of electrons plus localized-spins, the quantum dynamics of localized spins is always highly inhomogeneous and, therefore, quite different from the macrospin approximation [10] or simple spin wave excitations [24] assumed in the modeling of classical magnetization dynamics due to conventional STT.

*Global entanglement growth.*—Finally, we analyze entanglement growth [25] in Fig. 6(e) by computing time evolution of the so-called Meyer-Wallach measure [26] of global entanglement [27] defined for a multipartite quantum system composed of two-level subsystems as

$$Q_{\text{MW}} = 2 \left( 1 - \frac{1}{N_{\text{FM}} + N_e} \left[ \sum_{i=1}^{N_{\text{FM}}} \text{Tr} \hat{\rho}_i^2 + \sum_{j=1}^{N_e} \text{Tr} \hat{\rho}_{e,j}^2 \right] \right). \quad (7)$$

This measure quantifies average entanglement of each spin subsystem with the remaining  $N_{\text{FM}} + N_e - 1$  spins. It is invariant under local unitary transformations and it does not increase on average under local quantum operations and classical communication. Massively and long-range entangled many-body quantum states have been sought among ground states of exotic phases of condensed matter [28–30], and entanglement growth has been measured recently in few-qubit systems [25]. Conversely, in Fig. 6(e) nonequilibrium dynamics driven by quantum STT and local interactions in the Hamiltonian in Eq. (1) conspire to increase  $Q_{\text{MW}}(t) \rightarrow 0.93$  toward the max-

imum value but in a mundane FM material. It stays slightly below maximum  $Q_{\text{MW}} = 1$  because of initial  $s_e^z + S_{\text{spins}}^z \neq 0$ . Note that  $Q_{\text{MW}} = 1$  implies  $\mathbf{S}_i \equiv 0$ , as in quantum spin liquids [29, 30], which could happen for  $N_e = N_{\text{FM}}$  as demonstrated (solid black line) in Fig. 6(e). In contrast,  $Q_{\text{MW}}(t) \rightarrow 0.37$  reaches much smaller asymptotic value [Fig. 6(e)] in the case of conventional STT, so that  $Q_{\text{MW}}$  can be used to differentiate between quantum and classical STT in the case of coherent many-body dynamics of electrons plus localized-spins system.

We propose that by injecting an electron current of sufficient density, entanglement of macroscopically large number of flowing and localized spins can be detected by observing a magnetization reversal in collinear spin valves or magnetic tunnel junction, where the reversed magnetization of the FM-analyzer layer should be smaller than the one in equilibrium. Beyond spintronics, STT-driven quantum dynamics of localized spins can be employed to manipulate individual spin qubits and entangle them over long distances [31].

M. D. P. and P. P. were supported by ARO MURI Award No. W911NF-14-0247. A. E. F. acknowledges support by the US Department of Energy (DOE), Office of Science, Basic Energy Sciences (BES) Grant No. DE-SC0019275. B. K. N. was supported by NSF Grant No. ECCS 1922689.

---

\* [bnikolic@udel.edu](mailto:bnikolic@udel.edu)

- [1] D. Ralph and M. Stiles, Spin transfer torques, *J. Magn. Magn. Mater.* **320**, 1190 (2008).
- [2] N. Locatelli, V. Cros, and J. Grollier, Spin-torque building blocks, *Nat. Mater.* **13**, 11 (2014).
- [3] J. C. Slonczewski, Current-driven excitation of magnetic multilayers, *J. Magn. Magn. Mater.* **159**, L1 (1996).
- [4] L. Berger, Emission of spin waves by a magnetic multilayer traversed by a current, *Phys. Rev. B* **54**, 9353 (1996).
- [5] A. Zhodud, R. Freeman, R. Cao, A. Srivastava, and S. Urazhdin, Spin transfer due to quantum magnetization fluctuations, *Phys. Rev. Lett.* **119**, 257201 (2017).
- [6] S. Zhang, Viewpoint: quantum spin torque, *Physics* **10**, 135 (2017).
- [7] M. O. A. Ellis, M. Stamenova, and S. Sanvito, Multiscale modeling of current-induced switching in magnetic tunnel junctions using *ab initio* spin-transfer torques, *Phys. Rev. B* **96**, 224410 (2017).
- [8] K. Dolui, M. D. Petrović, K. Zollner, P. P. Plecháč, J. Fabian and B. K. Nikolić, First-principles theory of proximity spin-orbit torque on a two-dimensional magnet: Current-driven antiferromagnet-to-ferromagnet reversible transition in bilayer  $\text{CrI}_3$ , [arXiv:1909.13876](https://arxiv.org/abs/1909.13876) (2019).
- [9] M. D. Petrović, B. S. Popescu, U. Bajpai, P. Plecháč, and B. K. Nikolić, Spin and charge pumping by a steady or pulse-current-driven magnetic domain wall: A self-consistent multiscale time-dependent quantum-classical hybrid approach, *Phys. Rev. Applied* **10**, 054038 (2018).
- [10] D. V. Berkov and J. Miltat, Spin-torque driven magnetization dynamics: Micromagnetic modeling, *J. Magn. Magn. Mater.* **320**, 1238 (2008).
- [11] A. Qaiumzadeh and A. Brataas, Quantum magnetization fluctuations via spin shot noise, *Phys. Rev. B* **98**, 220408(R) (2018).
- [12] S. A. Bender, R. A. Duine, and Y. Tserkovnyak, Quantum spin-transfer torque and magnon-assisted transport in nanostructures, *Phys. Rev. B* **99**, 024434 (2019).
- [13] P. Mondal, U. Bajpai, M. D. Petrović, P. Plecháč, and B. K. Nikolić, Quantum spin transfer torque induced nonclassical magnetization dynamics and electron-magnetization entanglement, *Phys. Rev. B* **99**, 094431 (2019).
- [14] A. E. Feiguin, The density matrix renormalization group and its time-dependent variants, in A. Avella and F. Mancini (eds.), *AIP Conference Proceedings* **1419** (2011).
- [15] S. R. White and A. E. Feiguin, Real-time evolution using the density matrix renormalization group, *Phys. Rev. Lett.* **93**, 076401 (2004).
- [16] A. J. Daley, C. Kollath, U. Schollwöck, and G. Vidal, Time-dependent density-matrix renormalization-group using adaptive effective Hilbert spaces, *J. Stat. Mech. Theor. Exp.* **2004**, P04005 (2004).
- [17] S. Paeckel, T. Köhler, A. Swoboda, S. R. Manmana, U. Schollwöck, and C. Hubig, Time-evolution methods for matrix-product states, *Ann. of Phys.* **411**, 167998 (2019).
- [18] A. M. Tsvelik and O. M. Yevtushenko, Chiral spin order in Kondo-Heisenberg systems, *Phys. Rev. Lett.* **119**, 247203 (2017).
- [19] See Supplemental Material at <https://wiki.physics.udel.edu/qttg/Publications> for a movie which animates (for two different values of  $J_{sd}$ ) Figs. 3 and 4. It depicts time dependences  $\mathbf{S}_1(t), \dots, \mathbf{S}_5(t)$  for all five localized spins, as well as time evolution  $\mathbf{s}_i(t)$  of spin density at site  $i$  generated by electrons injected into the FM region in Fig. 2. The FM region of localized spins in the movies is denoted by gray rectangle. Electrons are initially ( $t < 0$ ) spin-polarized along the  $+z$ -axis, while localized spins are polarized along the  $-z$ -axis. The bottom panels in the movie show time evolution of charge density as it spreads from the region of  $N_{\text{conf}}$  sites in Fig. 2(a) into the FM region, thereby animating Fig. 3(a).
- [20] B. S. Shastri and D. C. Mattis, Theory of the magnetic polaron, *Phys. Rev. B* **24**, 5340 (1981).
- [21] A. Ekert and P. L. Knight, Entangled quantum systems and the Schmidt decomposition, *Am. J. Phys.* **63**, 415 (1995).
- [22] J. Kayser, K. Luoma, and W. T. Strunz, Geometric characterization of true quantum decoherence, *Phys. Rev. A* **92**, 052117 (2015).
- [23] S. Wang, Y. Xu, and K. Xia, First-principles study of spin-transfer torques in layered systems with noncollinear magnetization, *Phys. Rev. B* **77**, 184430 (2008).
- [24] A. Brataas, Y. Tserkovnyak, and G. E. W. Bauer, Current-induced macrospin versus spin-wave excitations in spin valves, *Phys. Rev. B* **73**, 014408 (2006).
- [25] T. Brydges, A. Elben, P. Jurcevic, B. Vermersch, C. Maier, B. P. Lanyon, P. Zoller, R. Blatt, and C. F. Roos, Probing Rényi entanglement entropy via randomized measurements, *Science* **364**, 260 (2019).
- [26] D. A. Meyer and N. R. Wallach, Global entanglement in

- multiparticle systems, J. Math. Phys. **43**, 4273 (2002).
- [27] A. Chandran, D. Kaszlikowski, A. Sen(De), U. Sen, and V. Vedral, Regional versus global entanglement in resonating-valence-bond states, Phys. Rev. Lett. **99**, 170502 (2007).
  - [28] B. Zeng, X. Chen, D.-L. Zhou, X.-G. Wen, *Quantum Information Meets Quantum Matter: From Quantum Entanglement to Topological Phases of Many-Body Systems* (Springer-Verlag, New York, 2019).
  - [29] C. Broholm, R. J. Cava, S. A. Kivelson, D. G. Nocera, M. R. Norman, and T. Senthil, Quantum spin liquids, Science **367**, eaay0668 (2020).
  - [30] T. Grover, Y. Zhang, and A. Vishwanath, Entanglement entropy as a portal to the physics of quantum spin liquids, New J. Phys. **15**, 025002 (2013).
  - [31] A. Bou Comas, E. M. Chudnovsky, and J. Tejada, Manipulating quantum spins by spin-polarized current: An approach based upon  $\mathcal{PT}$ -symmetric quantum mechanics, J. Phys.: Condens. Matter **31**, 195801 (2019).